

Evolution of domain structure in Fe_3GeTe_2

Siqi Yin(尹思琪), Le Zhao(赵乐), Cheng Song(宋成), Yuan Huang(黄元), Youdi Gu(顾有地), Ruyi Chen(陈如意), Wenxuan Zhu(朱文轩), Yiming Sun(孙一鸣), Wanjun Jiang(江万军), Xiaozhong Zhang(章晓中), and Feng Pan(潘峰)

Citation: Chin. Phys. B, 2021, 30 (**2**): 027505. DOI: 10.1088/1674-1056/abd693
Journal homepage: http://cpb.iphy.ac.cn; http://iopscience.iop.org/cpb

What follows is a list of articles you may be interested in

Magnetic characterization of a thin $Co_2MnSi/L1_0$–MnGa synthetic antiferromagnetic bilayer prepared by MBE

Shan Li(黎姗), Jun Lu(鲁军)†, Si-Wei Mao(毛思玮), Da-Hai Wei(魏大海), and Jian-Hua Zhao(赵建华)
Chin. Phys. B, 2020, 29 (**10**): 107501. DOI: 10.1088/1674-1056/ab99ac

Two-dimensional XSe_2 (X=Mn, V) based magnetic tunneling junctions with high Curie temperature

Longfei Pan(潘龙飞), Hongyu Wen(文宏玉), Le Huang(黄乐), Long Chen(陈龙), Hui-Xiong Deng(邓惠雄), Jian-Bai Xia(夏建白), Zhongming Wei(魏钟鸣)
Chin. Phys. B, 2019, 28 (**10**): 107504. DOI: 10.1088/1674-1056/ab3e45

Thickness-dependent magnetic anisotropy in obliquely deposited Fe(001)/Pd thin film bilayers probed by VNA-FMR

Qeemat Gul, Wei He(何为), Yan Li(李岩), Rui Sun(孙瑞), Na Li(李娜), Xu Yang(杨旭), Yang Li(李阳), Zi-Zhao Gong(弓子召), Zong-Kai Xie(谢宗凯), Xiang-Qun Zhang(张向群), Zhao-Hua Cheng(成昭华)
Chin. Phys. B, 2019, 28 (**7**): 077502. DOI: 10.1088/1674-1056/28/7/077502

Thickness dependent manipulation of uniaxial magnetic anisotropy in Fe-thin films by oblique deposition

Qeemat Gul, Wei He(何为), Yan Li(李岩), Rui Sun(孙瑞), Na Li(李娜), Xu Yang(杨旭), Yang Li(李阳), Zi-Zhao Gong(弓子召), ZongKai Xie(谢宗凯), Xiang-Qun Zhang(张向群), Zhao-Hua Cheng(成昭华)
Chin. Phys. B, 2018, 27 (**9**): 097504. DOI: 10.1088/1674-1056/27/9/097504

Effect of flash thermal annealing by pulsed current on rotational anisotropy in exchange-biased NiFe/FeMn film

Zhen Wang(王振), Shi-Jie Tan(谭士杰), Jun Li(李俊), Bo Dai(代波), Yan-Ke Zou(邹延珂)
Chin. Phys. B, 2018, 27 (**8**): 087504. DOI: 10.1088/1674-1056/27/8/087504

RAPID COMMUNICATION

Evolution of domain structure in Fe_3GeTe_2*

Siqi Yin(尹思琪)[1], Le Zhao(赵乐)[2], Cheng Song(宋成)[1,†], Yuan Huang(黄元)[3], Youdi Gu(顾有地)[1], Ruyi Chen(陈如意)[1], Wenxuan Zhu(朱文轩)[1], Yiming Sun(孙一鸣)[1], Wanjun Jiang(江万军)[2], Xiaozhong Zhang(章晓中)[1,‡], and Feng Pan(潘峰)[1]

[1] *Key Laboratory of Advanced Materials (MOE), School of Materials Science and Engineering, Tsinghua University, Beijing* 100084, *China*
[2] *State Key Laboratory of Low-Dimensional Quantum Physics and Department of Physics, Tsinghua University, Beijing* 100084, *China*
[3] *Institute of Physics, Chinese Academy of Sciences, Beijing* 100190, *China*

(Received 20 November 2020; revised manuscript received 15 December 2020; accepted manuscript online 24 December 2020)

Two-dimensional (2D) magnets provide an ideal platform to explore new physical phenomena in fundamental magnetism and to realize the miniaturization of magnetic devices. The study on its domain structure evolution with thickness is of great significance for better understanding the 2D magnetism. Here, we investigate the magnetization reversal and domain structure evolution in 2D ferromagnet Fe_3GeTe_2 (FGT) with a thickness range of 11.2–112 nm. Three types of domain structures and their corresponding hysteresis loops can be obtained. The magnetic domain varies from a circular domain via a dendritic domain to a labyrinthian domain with increasing FGT thickness, which is accompanied by a transition from squared to slanted hysteresis loops with reduced coercive fields. These features can be ascribed to the total energy changes from exchange interaction-dominated to dipolar interaction-dominated with increasing FGT thickness. Our finding not only enriches the fundamental magnetism, but also paves a way towards spintronics based on 2D magnet.

Keywords: Fe_3GeTe_2, two-dimensional magnet, thickness dependent domain structure

PACS: 75.70.Ak, 75.70.Kw **DOI:** 10.1088/1674-1056/abd693

1. Introduction

The two-dimensional (2D) van der Waals (vdW) magnet behaves as intrinsic ferromagnetic or antiferromagnetic states even when the thickness is reduced to a monolayer.[1–4] Recent discovery of 2D magnets such as CrI_3, $Cr_2Ge_2Te_6$, and Fe_3GeTe_2 (FGT) not only constitutes an ideal platform to explore the new physics of magnetism,[5,6,6–11] but also provides key materials for developing novel and high-performance spintronic devices.[12–14] Among these 2D materials, FGT emerges as an attractive candidate due to its metallic nature and relative high Curie temperature (∼220 K).[15–17] Its Curie temperature can be further enhanced to room temperature by effective modulation of Fe content,[18] ionic liquid,[16] ionic implantation,[19] exchange coupling,[20] and substrate.[21] Huge amount of interesting magnetic and transport properties have been discovered in FGT and its vdW heterostructure, large anomalous Hall effect,[16] Kondo lattice behavior,[22] large anomalous Nernst effect,[23] antisymmetric magnetoresistance,[24] stabilized magnetic skyrmion phase, etc.[25–27] Most recently, spin–orbit torque driven magnetization reversal has been achieved in FGT/Pt bilayers, showing a promising future towards spintronic applications based on 2D materials.[28]

Different from the bulk counterpart, it is natural to imagine the strong sensitivity of the performance of spintronics on the thickness of the 2D magnet. For example, a rich variety of domain structures in 2D FGT have been reported such as separated double-walled domain,[29] high-density Bloch-type skyrmion bubbles,[25] and movable Néel-type skyrmion state by current pulses.[26] When thinned down to a monolayer, FGT exhibits a strong perpendicular magnetic anisotropy. While a formation of labyrinthian domain pattern was observed in rather thicker FGT.[15,30] Previous studies provided a hint on the critical role of the film thickness on the performance of FGT-based devices. Besides the labyrinthian domain reported in previous studies,[15,27] we found that there also exists other configuration of magnetic domain in FGT such as circular and dendritic shape. There is a transition of magnetic domains from a circular domain via a dendritic domain then to a labyrinthian domain with increasing FGT thickness, which is accompanied by rich variation of magnetization reversal.

2. Experimental details

FGT was obtained by Au-assisted mechanical exfoliation method.[31,32] The thickness of FGT was estimated roughly based on its optical contrast and measured accurately by atomic force microscope (Fig. S1 and Table S1 in supplementary material). A commercial polar magneto-optical Kerr microscope (MOKE) was used to observe the magnetic domain of FGT at low temperature.

*Project supported by the National Key R&D Program of China (Grant Nos. 2017YFA0206202 and 2019YFA0308000), the National Natural Science Foundation of China (Grant Nos. 51871130, 62022089, and 11874405), and the Youth Innovation Promotion Association of Chinese Academy of Sciences (Grant No. 2019007).

†Corresponding author. E-mail: songcheng@mail.tsinghua.edu.cn
‡Corresponding author. E-mail: xzzhang@tsinghua.edu.cn

© 2021 Chinese Physical Society and IOP Publishing Ltd

3. Results and discussion

The crystal structure of monolayer FGT viewed from *xz* and *xy* planes is shown in the inset of Fig. 1. FGT can be regarded as a hexagonal layered vdW crystal with space group $P6_3/mmc$. FGT monolayer is composed of a Fe_3Ge covalently bonded slab sandwiched by two Te layers, and the Fe_3Ge slab consists of two Fe_I (valence state of Fe^{3+}) and one Fe_{II} (valence state of Fe^{2+}). The thickness of monolayer FGT is 0.8 nm with an interlayer vdW gap of 0.295 nm.[16]

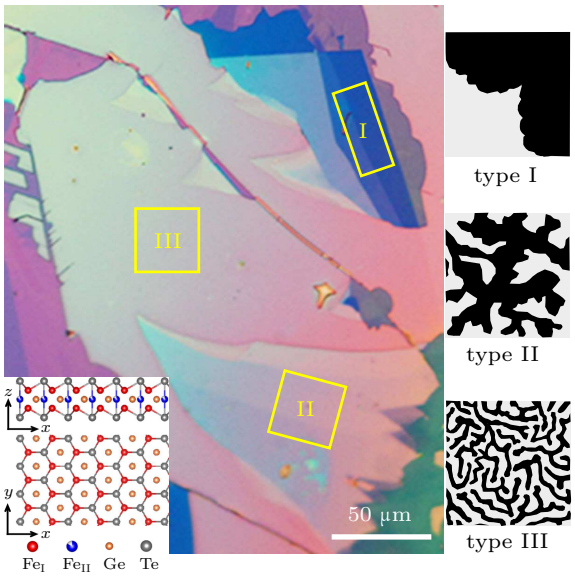


Fig. 1. Optical micrograph of FGT with different thicknesses and its corresponding domain structures. The regions I, II, and III in the left panel denote FGT with different thicknesses, and their corresponding typical magnetic domain structures are depicted as type I, type II, and type III in the right panel, respectively. The inset figure is the atomic structure of monolayer FGT viewed from *xz* and *xy* planes. Fe_I and Fe_{II} denote the two inequivalent Fe sites in the +3 and +2 states, respectively.

The optical micrograph of FGT with different thicknesses is displayed in the left panel of Fig. 1. FGT is divided into three regions by thickness. Regions I, II, and III are FGT crystals with thickness ranges of 11.2–21.6 nm, 25.6–40.8 nm, and 45.6–112 nm, respectively. The thickness of 2D FGT could be estimated roughly by optical microscopy where thinner FGT exhibits a blue contrast due to the high transparency.[33] The typical magnetic domain structures of FGT in regions I, II and III are identified as types I, II, and III, respectively [right panel of Fig. 1(a)]. The magnetic domain of type I which exists in the thinner FGT of 11.2–21.6 nm (such as region I) is a circular-shape domain. The case turns out to be different in type III which exists in the FGT thicker than 45.6 nm (such as region III), it is a multidomain with labyrinthian internal structure. As for type II, it is an intermediate case between type I and type III. The domain structure of type II is a dendritic multidomain, and its thickness range is between 25.6 nm and 40.8 nm. As for the FGT with the thicknesses of 21.6–25.6 nm and 40.8–45.6 nm, it shows a gradual transition from type I to type II and from type II to type III, respectively. The evolution of domain structure and magnetization reversal with thickness will be discussed below in detail.

Various domain structures correspond to different kinds of magnetization reversals and hysteresis loops. We focus now on type I, a thinner FGT with a thickness range of 11.2–21.6 nm. Optical micrography of region I is displayed in Fig. 2(a), and locations 1–4 present four FGT crystals of successive decreasing thickness. Figures 2(b)–2(e) are the hysteresis loops at locations 1–4, respectively, and it shows the change of Kerr signal in FGT sample at 150 K when the applied perpendicular magnetic field ($\mu_0 H_z$) sweeps from −57.9 mT to 57.9 mT, and back to −57.9 mT. A coercive field of 14 mT is observed in the hysteresis loop of location 1 [Fig. 2(b)]. When the thickness decreases, it shows an increase of coercive field to 23.3 mT and a change of hysteresis into a rectangular shape at location 2, indicating a stronger perpendicular magnetic anisotropy in a thinner film [Fig. 2(c)]. With further decreasing thickness, the coercive field becomes larger and reaches 43.4 mT at location 3 [Fig. 2(d)]. At location 4 with the thinnest thickness, the coercive field is larger than the limit of the magnetic field in polar magneto-optical Kerr effect, in this situation magnetization does not saturate [Fig. 2(e)]. Next, we observe the change in domain while the perpendicular magnetic field changes from 57.9 mT to −57.9 mT. The MOKE image of locations 1–4 at $\mu_0 H_z = 57.9$ mT is displayed in Fig. 2(f). The optical contrast of the MOKE images from white (location 1) to light grey (location 2) to dark grey (location 3) to black (location 4) shows a decrease in thickness. When the applied $\mu_0 H_z$ reaches −16.5 mT, the switching of domain at location 1 is firstly observed [Fig. 2(g)]. Then the field of −26.4 mT motivates the switching of domain in location 2 [Fig. 2(h)]. With further increasing $\mu_0 H_z$, the domain of location 3 reverses at −45.8 mT [Fig. 2(i)]. While it increases to −57.9 mT at last, partial reversal of magnetic domain in location 4 is observed [Fig. 2(j)]. These features suggest that the reversal of domain firstly occurs in the FGT with thicker thickness, then the thinner one, and it is consistent with the decrease of the coercive field with increasing thickness as illustrated in Figs. 2(b)–2(e). The dynamic process of domain reversal in this area also supports this point (video S1). Note that the domains in locations 3 and 4 are domains with circular shape (type I). The domain with circular shape is unstable and evolves to a completely inverted magnetization state spontaneously, thus inducing a rectangular hysteresis loop with no gradual change. Since the domain width increases exponentially with thickness,[34] a single domain is expected to be observed in the thinnest sample, when the domain width exceeds the sample size.

Figure 3(a) is the hysteresis loop of FGT containing locations 1–4 measured at 175 K, showing it having four steps labeled as 1–4, corresponding to the magnetization reversals

of locations 1–4, respectively. A similar case can also be observed in the hysteresis loop measured at 150 K that four steps exist in the hysteresis loop but its shape changes due to decreasing temperature [Fig. 3(b)]. The magnetic field of steps 1–4 corresponds to the coercive field of locations 1–4 in Figs. 2(b)–2(e), respectively. It explains that the hysteresis loop of 2D magnet sometimes is found to have many steps, due to the inhomogeneity thickness in the measured 2D magnet. In the same way, the two steps of the loop in Fig. 2(d) could be attributed to the selected area having drifted away and contained a small part of location 2 when measuring the Kerr loop.

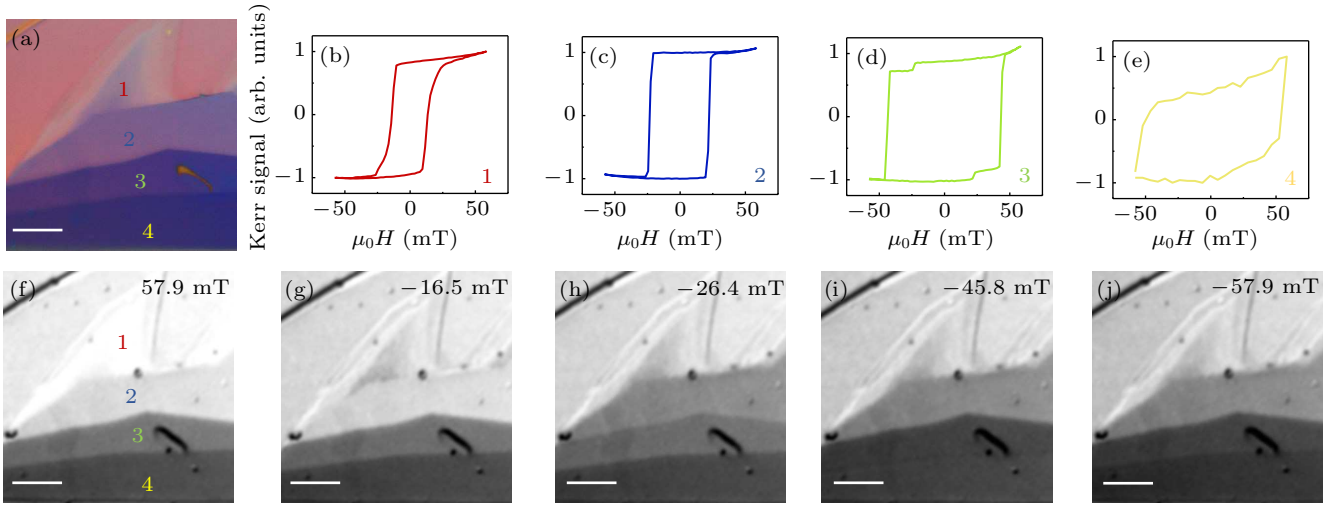


Fig. 2. Hysteresis loop and domain structure of FGT in type I. (a) Optical micrography of FGT in type I. Locations 1–4 are FGT crystals with decreasing thickness. (b)–(e) Hysteresis loops of locations 1–4 measured by MOKE at 150 K, respectively. MOKE images of FGT at locations 1–4 under different perpendicular magnetic field: (f) +57.9 mT, (g) −16.5 mT, (h) −26.4 mT, (i) −45.8 mT, and (j) −57.9 mT. Scale bar is 25 μm.

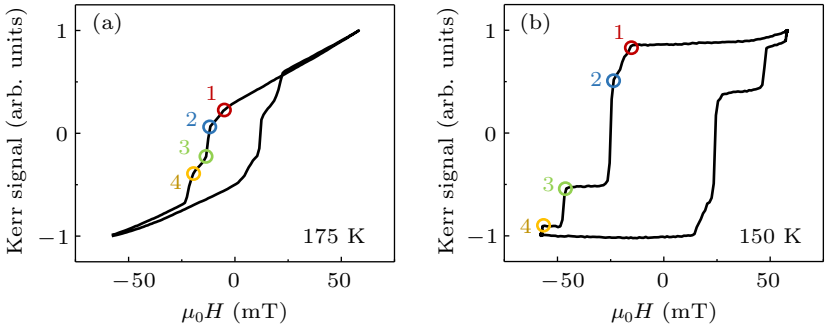


Fig. 3. Hysteresis loop of FGT containing locations 1–4 measured by MOKE at different temperature: (a) 175 K, (b) 150 K.

We now turn towards region II. The corresponding data are presented in Fig. 4. The typical MOKE images of domain in region II show a dendritic structure [Fig. 4(a)]. Concomitant MOKE images of region II are displayed in Fig. 4(e). Locations 5–7 are three FGT crystals in region II with thicknesses of 40.8 nm, 32 nm, 28.8 nm, and their hysteresis loops are illustrated in Figs. 4(b)–4(d), respectively. Here, the hysteresis loop of region II has a smaller coercivity than that of region I, and a gradual inversion of magnetization begins when $\mu_0 H_z$ reaches the coercive field, resembling to hourglass-shape. As $\mu_0 H_z$ is swept from 57.9 mT to −57.9 mT, nucleation field H_N is defined as a field when the magnetization begins to drop rapidly.[35,36] As depicted in Fig. 4(b), the Kerr signal has a sharp decrease at nucleation field H_N and then gradually decreases to reach the magnetization saturation, revealing the existence of multidomain. This is quite different from the type I having a circular domain with a rectangular loop. The coercive fields of locations 5–7 are 10 mT, 15.2 mT, and 17.9 mT, respectively, demonstrating once again that it increases with decreasing thickness. Then a domain variation of region II is recorded during field sweeping from 57.9 mT to −57.9 mT. The reversal of magnetic domain occurs in location 5 when $\mu_0 H_z$ reaches −11.5 mT [Fig. 4(f)], and then in location 6 at the field of −16.5 mT [Fig. 4(g)], followed by in location 7 at the field of −18.6 mT [Fig. 4(h)]. This sequence of magnetization reversal is supported by the dynamic process of domain change (video S2). The magnetic domain in region II is dendritic, and grows from one side to take over the whole FGT crystals with variation of $\mu_0 H_z$. Besides, it is not difficult to find that the domain size has a close relationship with the thickness. The domain size gradually increases from location 5 to location 6 then to location 7, reflecting an increasing tendency of the domain size with decreasing thickness.

In the following we discuss the magnetization in region

III and its domain structure type III. Region III represents the thick FGT with a thickness larger than 45.6 nm. A typical hysteresis loop of type III domain shows seriously reduced coercivity and remanence, which features as a tilted hourglass, as illustrated in Fig. 5(a). Compared to that in type II, the hysteresis loop of type III shown in Fig. 5(a) has three notable features. Firstly, different from a negative H_N of type II, the nucleation field of type III is positive accompanied by a gradual drop of magnetization at H_N. As the FGT thickness of type III increases, the positive nucleation field gradually increases (Fig. S2). It indicates a decreasing impedance for domain wall nucleation and motion with increasing film thickness.[37] Secondly, a big difference is seen in the remanence. The hysteresis loop of type II reveals a remanence of almost 100%, and that of type III exhibits an extreme small remanence at zero field. Thirdly, unlike a sharp change at H_N in type II, the reversal of magnetization in type III occurs gradually. In addition, the hysteresis loop of type III does not have a variation from rectangular to irregular with increasing thickness, which is different from that of types I and II. The magnetic domain in region III emerges as the labyrinthian domain. With $\mu_0 H_z$ varying from 57.9 mT to −57.9 mT, the labyrinthian domain appears as the field reaches 27.9 mT, leading to the drop of magnetization at H_N, as displayed in Fig. 5(b). As the field further decreases, the amount of labyrinthian domain increases [Fig. 5(c)]. With further decrease of $\mu_0 H_z$, the density of the labyrinthian domain increases until the magnetization inverts completely [Fig. 5(d)]. The remanence of nearly zero observed in Fig. 5(a) can be explained as equal width of up and down stripe-domains at zero field. The above discussion can be also confirmed by the dynamic process of domain reversal in region III (video S3). The amount of labyrinthian domain gradually increases with the variation of the magnetic field until it reaches magnetization saturation.

The labyrinthian magnetic domain (type III) in thicker FGT has also been verified by magnetic force microscopy and Lorentz transmission electron microscopy in previous studies.[15,27] On basis of this, we find that the magnetic domain of FGT also has circular (type I) and dendritic (type II) shapes. It can be clearly figured out that the thickness ranges of type I, type II, and type III domain are 11.2–21.6 nm, 25.6–40.8 nm, and 45.6–112 nm, respectively (Table S1). Figure 6 summarizes the evolution of domain structure and its corresponding hysteresis loop with FGT thickness at 150 K, demonstrating that both the domain size and coercive field decrease with increasing FGT thickness. This evolution of magnetic domain in FGT shares similar characteristic with the Co/Pt multilayer with low disorder.[38] Further modulation of magnetic domain in FGT can be expected through electric field control in the next step.[39]

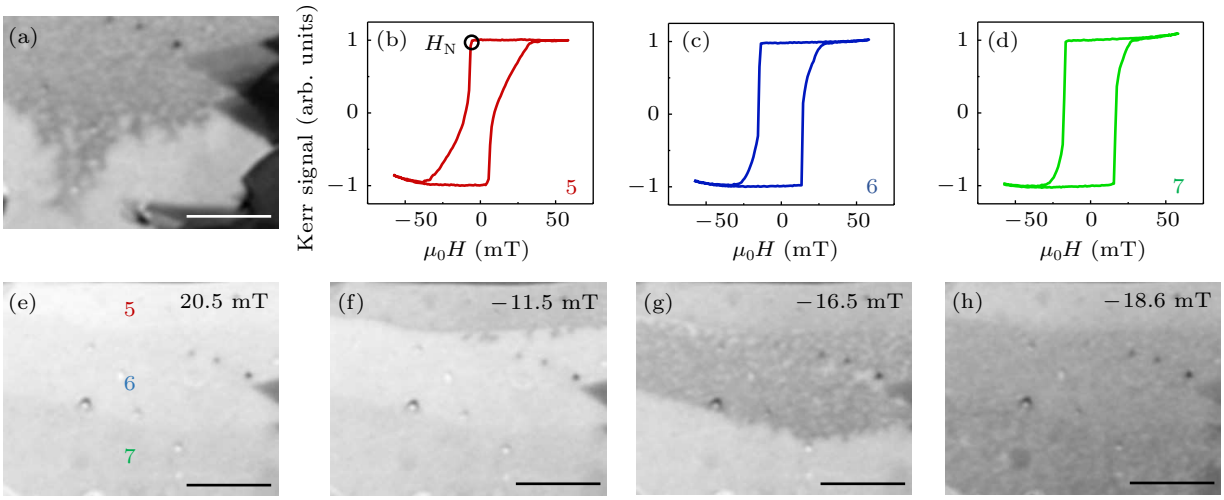


Fig. 4. Hysteresis loop and domain structure of FGT in type II. (a) MOKE images of domain structure of FGT in type II. Locations 5–7 are FGT crystals with successive decreasing thickness. (b)–(d) Hysteresis loops of locations 5–7 measured by MOKE at 150 K, respectively. MOKE images of FGT at locations 5–7 under different perpendicular magnetic field: (e) +20.5 mT, (f) −11.5 mT, (g) −16.5 mT, and (h) −18.6 mT. Scale bar is 25 μm.

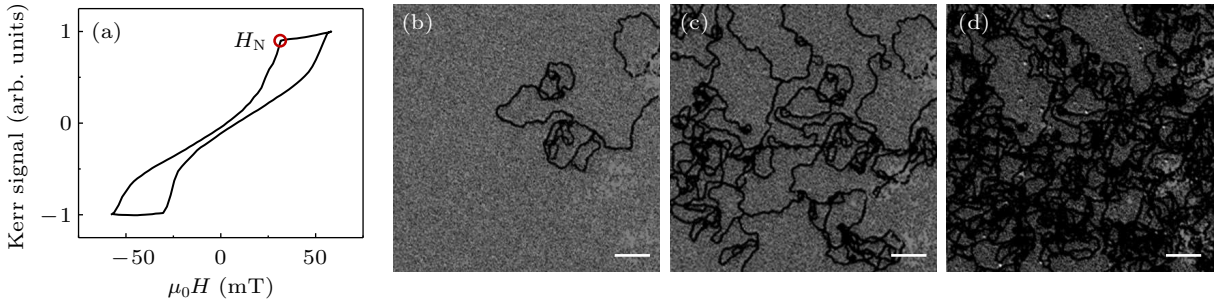


Fig. 5. Hysteresis loop and domain structure of FGT in type III. (a) Hysteresis loop of FGT in type III measured by MOKE. MOKE images of FGT in type III under different perpendicular magnetic field: (b) +27.9 mT, (c) +27.6 mT, and (d) +26.7 mT. A background was subtracted for the MOKE image. Scale bar is 25 μm.

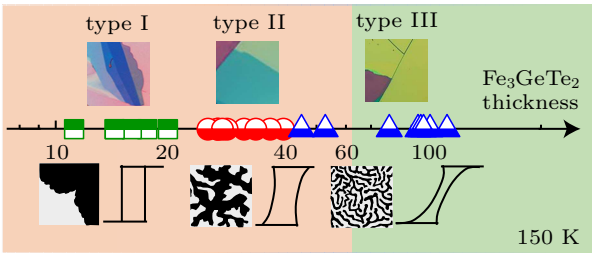


Fig. 6. The evolution of magnetic domain structure and hysteresis loop in Fe_3GeTe_2 at 150 K.

We then propose a simple model to explain the thickness dependent domain configurations. The total energy of the FGT sample with a thickness of t can be expressed as[36]

$$E = E_{\rm w} + E_{\rm d} + E_{\rm u} = \gamma_{\rm w} S - \frac{1}{2}\int (M \cdot H)\,{\rm d}V + K_{\rm u} V_{\rm u}, \quad (1)$$

where $E_{\rm w}$, $E_{\rm d}$, and $E_{\rm k}$ are the domain wall energy, stray field energy, and anisotropy energy of samples, respectively. Domain wall energy $E_{\rm w}$ is equal to the product of domain wall energy per unit area ($\gamma_{\rm w}$) and total surface area of the domain wall (S). The stray field energy $E_{\rm d}$ is determined by the integral of magnetization M and magnetic field H. Anisotropy energy $E_{\rm u}$ can be expressed by the multiply of uniaxial magnetic anisotropy $K_{\rm u}$ and volume of domains not oriented in the easy direction $V_{\rm u}$.

The configurations of magnetic domain with uniaxial anisotropy can be simply divided into cases A, B, and C, as displayed in Fig. 7(a). Case A is a single domain with a spin orientation along the easy axis, while case B shows a multidomain and its cross-section is a rectangular domain with alternate spin orientations. As for case C, it presents a closure multidomain with a spin flux closure within the film. The domain width of the multidomain is assumed to be d. The totally energy per unit area of cases A, B, and C is calculated as following. For case A of single domain, total free energy E arises from the stray field energy $E_{\rm d}$, which is given by

$$E = E_{\rm d} = \frac{1}{2}\mu_0 M_{\rm s}^2 t, \quad (2)$$

where μ_0 is the permeability of vacuum and $M_{\rm s}$ is the saturation magnetization of the film. As for case B, total free energy E is a sum of stray field energy $E_{\rm d}$ and domain wall energy $E_{\rm w}$, which can be expressed as

$$E = E_{\rm d} + E_{\rm w} = 1.7 \times 10^{-7} M_{\rm s}^2 d + \gamma_{\rm w} \frac{t}{d}. \quad (3)$$

Total free energy E reaches the minimum when $\partial E/\partial d = 0$ and $d = \frac{10^4}{M_{\rm s}}\sqrt{\frac{\gamma_{\rm w} t}{17}}$, and it is $E_{\rm min} = 2M_{\rm s}\sqrt{17\gamma_{\rm w} t} \times 10^{-4}$.

Case C is the multidomain with closure configuration which is formed to decrease the stray field energy. We have

$$E = E_{\rm w} + E_{\rm k} = \frac{2\sqrt{2}d + t - d}{d}\gamma_{\rm w} + \frac{1}{2}d^2 K_{\rm u}. \quad (4)$$

This is minimum for $\partial E/\partial d = 0$ and $d = \sqrt{2\gamma_{\rm w} t/K_{\rm u}}$, giving $E_{\rm min} = (2\sqrt{2} - 1)\gamma_{\rm w} + \sqrt{2\gamma_{\rm w} K_{\rm u} t}$. The variation of total free energy E with film thickness t is plotted in Fig. 7(b), and we take the parameters of bulk FGT as $M_{\rm s} = 376$ emu/cm^3, $\gamma_{\rm w} = 4.7\,{\rm erg/cm^2}$, and $K_{\rm u} = 1.46 \times 10^7$ erg/cm^3.[40] It shows that the total free energy of case A is the smallest when thickness t is less than 57.3 nm, which reveals that FGT of thinner thickness less than 57.3 nm tends to form a single domain configuration. Once the film thickness t is larger than 57.3 nm, the total energy of case B becomes the lowest. As the film thickness increases, the magnetic domain transforms from single domain (case A) to multidomain (case B) accompanied by generation of domain wall and decrease of domain width, which is in accordance with the experimental results we observed. The critical thickness 57.3 nm between single domain and multidomain by calculation is quite larger than the experimental observation (less than 11.2 nm at least), and it may result from the parameters we used in calculation which were obtained in bulk FGT.[40] The total energy of FGT in case C is quite high compared with cases A and B, so it cannot exist in FGT films. The domain wall energy is determined by the exchange interaction and anisotropy coefficient, whereas the stray field energy originates from the dipolar–dipolar interaction. The exchange interaction and perpendicular magnetic anisotropy favor a parallel alignment of spins in perpendicular direction and a formation of single domain in ferromagnetic FGT. The dipolar interaction favors opposite alignment of spins and forms a stripe domain to decrease the stray field.[41] A variation from single domain to multidomain structure indicates a crossover of the total energy from exchange interaction-dominated to dipolar interaction-dominated.[42–44]

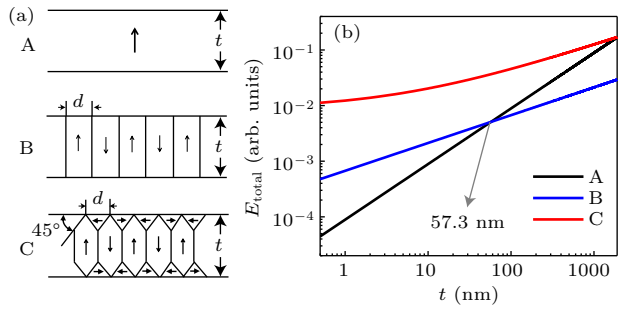


Fig. 7. Domain configuration and its thickness dependence. (a) Domain configurations of cases A, B, and C. The domain width and film thickness are denoted as d and t, respectively. (b) Energy of domain configurations A, B, C varies with thickness.

4. Conclusion

We have investigated the thickness dependent evolution of domain structure in FGT. The domain of FGT transforms from circular magnetic domain to dendritic multidomain to labyrinthian domain with increasing thickness. Both domain size and coercive field of FGT are also found to decrease with the increase in thickness. The evolutions of the domain can be ascribed to energy changes from exchange interaction-dominated in thinner layers to dipolar interaction-dominated

in thicker layers. Our findings disclose an interesting evolution of domain configuration in FGT.

Acknowledgment

The authors thank Bolun Wang for help in AFM measurement. C.S. acknowledges the support of Beijing Innovation Center for Future Chip (ICFC), Tsinghua University.

References

[1] Gong C and Zhang X 2019 *Science* **363** eaav4450
[2] Burch K S, Mandrus D and Park J G 2018 *Nature* **563** 47
[3] Gibertini M, Koperski M, Morpurgo A F and Novoselov K S 2019 *Nat. Nanotechnol.* **14** 408
[4] Sun X, Zhao S, Bachmatiuk A, Rummeli M H, Gorantla S, Zeng M and Fu L 2020 *Small* **16** 2001484
[5] Purbawati A, Coraux J, Vogel J, Hadj-Azzem A, Wu N, Bendiab N, Jegouso D, Renard J, Marty L, Bouchiat V, Sulpice A, Aballe L, Foerster M, Genuzio F, Locatelli A, Mentes T, Han Z, Sun X, Nunez-Regueiro M and Rougemaille N 2020 *ACS Appl. Mater. Interfaces* **12** 30702
[6] Huang B, Clark G, Moratalla E N, Klein D R, Cheng R, Seyler K L, Zhong D, Schmidgall E, McGuire M A, Cobden D H, Yao W, Xiao D, Herrero P J and Xu X. 2017 *Nature* **546** 270
[7] Wang Z, Zhang T, Ding M, Dong B, Li Y, Chen M, Li X, Huang J, Wang H, Zhao X, Li Y, Li D, Jia C, Sun L, Guo H, Ye Y, Sun D, Chen Y, Yang T, Zhang J, Ono S, Han Z and Zhang Z 2018 *Nat. Nanotechnol.* **13** 554
[8] Li T, Jiang S, Sivadas N, Wang Z, Xu Y, Weber D, Goldberger J E, Watanabe K, Taniguchi T, Fennie C J, Mak K F and Shan J 2019 *Nat. Mater.* **18** 1303
[9] Chen W, Sun Z, Wang Z, Gu L, Xu X, Wu S and Gao C 2019 *Science* **366** 983
[10] Kim H H, Jiang S, Yang B, Zhong S, Tian S, Li C, Lei H, Shan J, Mak K F and Tsen A W 2020 *Adv. Mater.* **32** 1905433
[11] Wang Y M, Tian S J, Li C H, Jin F, Ji J T, Lei H C and Zhang Q M 2020 *Chin. Phys. B* **29** 056301
[12] Song C, Zhang R, Liao L, Zhou Y, Zhou X, Chen R, You Y, Chen X and Pan F 2020 *Prog. Mater. Sci.* https://doi.org/10.1016/j.pmatsci.2020.100761
[13] Lin H, Yan F, Hu C, Lv Q, Zhu W, Wang Z, Wei Z, Chang K and Wang K 2020 *ACS Appl. Mater. Interfaces* **12** 43921
[14] Song T, Cai X, Tu M W Y, Zhang X, Huang B, Wilson N, Seyler K L, Zhu L, Taniguchi T, Watanabe K, McGuire M A, Cobden D H, Xiao D, Yao W and Xu X 2018 *Science* **360** 1214
[15] Fei Z, Huang B, Malinowski P, Wang W, Song T, Sanchez J, Yao W, Xiao D, Zhu X, May A F, Wu W, Cobden D H, Chu J H and Xu X 2018 *Nat. Mater.* **17** 778
[16] Deng Y, Yu Y, Song Y, Zhang J, Wang N Z, Sun Z, Yi Y, Wu Y Z, Wu S, Zhu J, Wang J, Chen X H and Zhang Y 2018 *Nature* **563** 94
[17] Wu Q, Ang Y S, Cao L and Ang L K 2019 *Appl. Phys. Lett.* **115** 083105
[18] May A F, Ovchinnikov D, Zheng Q, Hermann R, Calder S, Huang B, Fei Z, Liu Y, Xu X and McGuire M A 2019 *ACS Nano* **13** 4436
[19] Yang M, Li Q, Chopdekar R V, Stan C, Cabrini S, Choi J W, Wang S, Wang T, Gao N, Scholl A, Tamura N, Hwang C, Wang F and Qiu Z 2020 *Adv. Quantum Technol.* **3** 2000017
[20] Zhang L, Huang X, Dai H, Wang M, Cheng H, Tong L, Li Z, Han X, Wang X, Ye L and Han J 2020 *Adv. Mater.* **32** 2002032
[21] Zhang L, Song L, Dai H, Yuan J, Wang M, Huang X, Qiao L, Cheng H, Wang X, Ren W, Miao X, Ye L, Xue K and Han J 2020 *Appl. Phys. Lett.* **116** 042402
[22] Zhang Y, Lu H, Zhu X, Tan S, Feng W, Liu Q, Zhang W, Chen Q, Liu Y, Luo X, Xie D, Luo L, Zhang Z and Lai X 2018 *Sci. Adv.* **4** eaao6791
[23] Fang C, Wan C, Guo C, Feng C, Wang X, Xing Y, Zhao M, Dong J, Yu G, Zhao Y and Han X 2019 *Appl. Phys. Lett.* **115** 212402
[24] Albarakati S, Tan C, Chen Z, Partridge J G, Zheng G, Farrar L, Mayes E L, Field M R, Lee C, Wang Y, Xiong Y, Tian M, Xiang F, Hamilton A R, Tretiakov O A, Culcer D, Zhao Y and Wang L 2019 *Sci. Adv.* **5** eaaw0409
[25] Ding B, Li Z, Xu G, Li H, Hou Z, Liu E, Xi X, Xu F, Yao Y and Wang W 2020 *Nano Lett.* **20** 868
[26] Park T E, Peng L, Liang J, Hallal A, Yasin F S, Zhang X, Song K M, Kim S J, Kim K, Weigand M, Schutz G, Finizio S, Raabe J, Garcia K, Xia J, Zhou Y, Ezawa M, Liu X, Chang J, Koo H C, Kim Y D, Chshiev M, Fert A, Yang H, Yu X and Woo S 2019 ArXiv: 1907.01425
[27] Wu Y, Zhang S, Zhang J, Wang W, Zhu Y L, Hu J, Wong K, Fang C, Wan C, Han X, Shao Q, Taniguchi T, Watanable K, Mao Z, Zhang X and Wang K L 2020 *Nat. Commun.* **11** 3860
[28] Wang X, Tang J, Xia X, He C, Zhang J, Liu Y, Wan C, Fang C, Guo C, Yang W, Guang Y, Zhang X, Xu H, Wei J, Liao M, Lu X, Feng J, Li X, Peng Y, Wei H, Yang R, Shi D, Zhang X, Han Z, Zhang Z, Zhang G, Yu G and Han X 2019 *Sci. Adv.* **5** eaaw8904
[29] Nguyen G D, Lee J, Berlijn T, Zou Q, Hus S M, Park J, Gai Z, Lee C and Li A P 2018 *Phys. Rev. B* **97** 014425
[30] Tan C, Lee J, Jung S G, Park T, Albarakati S, Partridge J, Field M R, McCulloch D G, Wang L and Lee C 2018 *Nat. Commun.* **9** 1554
[31] Huang Y, Sutter E, Shi N N, Zheng J, Yang T, Englund D, Gao H J and Sutter P 2015 *ACS Nano* **9** 10612
[32] Huang Y, Pan Y H, Yang R, Bao L H, Meng L, Luo H L, Cai Y Q, Liu G D, Zhao W J, Zhou Z, Wu L M, Zhu Z L, Huang M, Liu L W, Liu L, Cheng P, Wu K H, Tian S B, Gu C Z, Shi Y G, Guo Y F, Cheng Z G, Hu J P, Zhao L, Yang G H, Sutter E, Sutter P, Wang Y L, Ji W, Zhou X J and Gao H J 2020 *Nat. Commun.* **11** 2453
[33] Li X L, Han W P, Wu J B, Qiao X F, Zhang J and Tan P H 2017 *Adv. Funct. Mater.* **27** 1604468
[34] Speckmann M, Oepen H P and Ibach H 1995 *Phys. Rev. Lett.* **75** 2035
[35] Jagla E A 2005 *Phys. Rev. B* **72** 094406
[36] Kittel C 1946 *Phys. Rev.* **70** 965
[37] Thiele J U, Folks L, Toney M F and Weller D K 1998 *J. Appl. Phys.* **84** 5686
[38] Pierce M S, Buechler C R, Sorensen L B, Turner J J, Kevan S D, Jagla E A, Deutsch J M, Mai T, Narayan O, Davies J E, Liu K, Hunter Dunn J, Chesnel K M, Kortright J B, Hellwig O and Fullerton E E 2005 *Phys. Rev. Lett.* **94** 017202
[39] Song C, Cui B, Peng J, Mao H and Pan F 2016 *Chin. Phys. B* **25** 067502
[40] León-Brito N, Bauer E D, Ronning F, Thompson J D and Movshovich R 2016 *J. Appl. Phys.* **120** 083903
[41] Won C, Wu Y, Choi J, Kim W, Scholl A, Doran A, Owens T, Wu J, Jin X, Zhao H and Qiu Z 2005 *Phys. Rev. B* **71** 224429
[42] Li Q, Yang M, Gong C, Chopdekar R V, N'Diaye A T, Turner J, Chen G, Scholl A, Shafer P, Arenholz E, Schmid A K, Wang S, Liu K, Gao N, Admasu A S, Cheong S W, Hwang C, Li J, Wang F, Zhang X and Qiu Z 2018 *Nano Lett.* **18** 5974
[43] Xie R, Wei J, Liu Z, Tang Y, Tang T, Tang S and Du Y 2014 *Chin. Phys. B* **23** 068103
[44] Zhang Z, Liu H and Han B 2002 *Chin. Phys.* **11** 629